



Geochemical Characteristics and Radioactive Elements Estimation along Trenches of Um Ara area, South Eastern Desert, Egypt

Saleh GM* and Kamar MS

Abstract

Um Ara area is located in the extreme south Eastern Desert of Egypt between 581400mE-584900mE and 2503000mN-2504600mN. The area comprises distinct tectono-stratigraphic units beginning with the oldest as follows: Dokhan volcanic and post-collision granitoids (monzogranite, and alkali feldspar granite), and associated with dykes and quartz veins. The granite affected by deuteric K-metasomatism (microclinization) followed by Na-metasomatism (albitization) causing zonation in this part of the pluton. The high radioactivity in the anomalous sites is structurally controlled (strong shearing, fracturing and jointing). The intensity of mineralization is especially significant along joint sets striking NNW-SSE, NNE-SSW and NE-SW trending. The spacing among these joints ranges from few mm up to about 5 cm. locally, the joints are filled with kaolinite and other alteration products including hematite and Mn-oxides. Geochemically, Um Ara granites trenches and core samples show a relative enrichment in K_2O compositions due to plagioclase destruction and formation of muscovite/sericitization.

Um Ara granites trenches and core samples have variable total REEs contents 117.41 to 308.28 and 256.51 to 397.22 ppm respectively. Σ LREEs in trenches and core samples range from 108.47 to 298.41 ppm and from 236.84 to 384.78 ppm respectively, whereas Σ HREEs range from 5.48 to 14.01 ppm and from 12.44 to 19.67 ppm respectively. The lowest concentration of total REEs in core samples is at 100m depth, while the highest values at 145m depth. Um Ara granites trenches, U contents vary from 154 to 506 ppm with an average of 245.7 ppm, and Th contents vary from 47 to 415 ppm with an average of 165.4 ppm. Core samples granite, U contents vary from 128 to 349 ppm with an average of 237.3 ppm, and Th contents vary from 45 to 146 ppm with an average 107.4 ppm. Visible secondary uranium mineralization is represented mainly by uranophane and β -uranophane. Uranium is also contained within a range of U-bearing accessory minerals, mainly fluorite, monazite, xenotime, allanite and zircon. The secondary processes played a main role in uranium enrichment (uranium added to these granitic sites post-magmatically). Um Ara altered granites trenches and core samples rocks are an abnormal radiation and have an extension. So, these anomalies are suitable to be a place for uranium extraction. The result is the continuous of its mining work besides leachability experiments.

Keywords

Radioactive minerals; Um Ara granites; Uranophane; Microclinization; Mining work; Egypt

Introduction

The Arabian-Nubian Shield (ANS) forms a suture between the East and West Gondwana at the northern end of the East African Orogen, which encompasses the ANS in the north and the Mozambique Belt in the south. The Arabian-Nubian Shield, covering large parts ($\sim 3 \times 10^6$ km²; Kusky et al. [1]) of NE Africa, Sinai and Arabia. It evolved during the Pan-African orogeny. It has been suggested that the evolution of the Arabian-Nubian Shield was neither entirely ensialic nor ensimatic, but it represents a complex amalgamation of arcs, oceanic plateaus and microcontinents assembled during Neoproterozoic closure of the Mozambique Ocean [2,3]. The evolution of the ANS encompasses four major tectono-magmatic episodes that occurred between 800 and 550 Ma [4]. These are: (1) rifting of the supercontinent Rodinia (~ 800 Ma; Kampunzu et al. [5]; Loizenbauer et al. [6].), (2) sea-floor spreading, arc and back arc basin formation, and accretion of the juvenile crust (870-690 Ma), (3) continental collision (750-650 Ma), and (4) east-west crustal shortening (640-550 Ma) when East and West Gondwana collided.

The Egyptian basement complex of the Eastern Desert (ED) and South Sinai constitutes its northwestern segment. The Arabian-Nubian Shield (ANS) is regarded the best preserved and largest-exposed area of Neoproterozoic juvenile continental crust on the Earth [7-9]. The ANS juvenile crust has evolved during most of the Neoproterozoic time (900-600 Ma; [4]).

Granitoid rocks in the Eastern Desert of Egypt have long been classified as syn- to late-orogenic granitoids (Older granitoids) and post-orogenic to anorogenic granites (Younger granites) [10-12]. The older granitoids range from quartz diorite to rare true granite (predominantly muscovite trondhjemite, tonalite, and granodiorite). These are I-type, subduction-related plutons, with ages between 870 and 614 Ma using Rb-Sr and U-Pb methods [2,13,14]. Younger granites are mainly monzogranites, syenogranites, and alkali-feldspar granites, I-type (partly subduction-related) but mainly alkaline to peralkaline A-type plutons, formed between 610 and 550 Ma based on the Rb-Sr and U-Pb dating [15] and developed during extension.

The Egyptian granitoids are of I- and A- type affinity, and were generated either by partial melting of mafic lower crust or by fractionation of a mantle-derived magma [14,17-19]. The younger granitoids are widely distributed in the Nubian Shield of Egypt, constituting approximately 30 % of its plutonic proportion [20]. Recently, El Sayed [16] classified the younger granitoids into orogenic I-type arc-related, orogenic A-type arc-related, and anorogenic A-type rift-related granites. Most of the geological work on the younger granitoids in Egypt dealt with the arc-related types and little attention has been given to the post-orogenic and anorogenic granitoids [21,22].

Alkali-metasomatism refers to the geological behavior by which alkali (K or Na)-rich hydrothermal fluids interact with the country

*Corresponding author: Saleh GM, Professor, Nuclear Materials Authority, El-Maadi, Cairo, Egypt. Tel: +20 502262562; E-mail: drgehad_m@yahoo.com

Received: February 19, 2018 Accepted: March 28, 2018 Published: April 04, 2018

rocks and form the altered rocks mainly composed of albite or potassium feldspar and accompanied by some other altered minerals. It is impossible for potassium and sodium in the nature to occur simultaneously in the hydrothermal fluids, the main alteration could be observed in alkali-metasomatism is single albitization or single feldsparization, when the albitization dominates, it could be called as alkali-metasomatism; when the feldsparization dominates, it could be called as potassium-metasomatism. Alkali-metasomatic type uranium deposit is one of the main industrial uranium deposits, has been discovered around the world [23]. K-metasomatism is characterized by replacement of sodic and calcic phases by potassic phases. Sometimes replacement of K instead of Na and Ca may accompanied by silicification and addition of metals and hydration.

The common Egyptian uranium occurrences are mainly: vein-type (G. El-Missikat [24], G. Sella [25,26]), metasomatised granites (G Um Ara [27]), shear zones in calc-alkaline granite (G Gattar [28]), two mica granites (G Nasb Aluba [29] and G Ribdab [30]) and shear zones hosted lamprophyre bearing-REEs and U in Abu Rusheid area [31]. Uranyl silicates are typical alteration phases of the primary uranium mineralization of the alteration zone of many uranium deposits. Uranyl silicate minerals are typical representatives of the long-term alteration products, indicating usually late stage, or the high-grade of weathering. Uranyl silicates, as uranophane and/or kasolite, are common constituents of massive aggregates of alteration phases, replacing primary uraninite in situ; aggregates of uranyl silicates occur often along with uranyl phosphates in the strongly oxidized portions of the primary mineralization [32].

Although previous investigations showed the presence of uraninite as a primary uranium mineral in the alkali-feldspar granites [33,27], more recent studies [35,36] reported only the occurrence of uranophane and β -uranophane as the main uranium minerals.

Abdel Naby et al. [37] suggested a two-stage metallogenetic model for the alteration processes and origin of U- and Th-bearing minerals

in Um Ara area: 1) the first stage was dominated by hydrothermal alteration and accompanied by albitization, k-feldspathization, desilicification, chloritization, hematitization, silicification, argillization, fluoritization and corrosion of primary U-bearing minerals. Solid-solution between thorite and zircon occurred during this stage. The second stage occurred by mobilizing the early formed primary U-bearing minerals near-surface by the action of meteoric water. Uranium was transported as a calcium uranyl carbonate complexes. When these complexes lost their stabilities by precipitation of calcite, they decomposed in the presence of silica to form uranophane.

The main objectives of this study were to investigate and determine the geochemical alteration processes along trenches and drilled borehole at the northwestern part of Um Ara granitic pluton, which is totally composed of fine grained alkali feldspar granites rich by uranium and thorium mineralization.

Geologic Setting and Petrography

The google earth image covers a major part of Um Ara area (Figure 1) was used for general rock type identification and association. From the studies of the different geological features, rock types, tectonics and mineralization of Um Ara area (Figure 2) can be classified into Dokhan volcanic and post-collision granitoids (monzogranite and alkali feldspar granite), and associated with dykes and quartz veins. The geology of Um Ara area has been extensively studied by many authors [27,33,38,40,64].

Dokhan volcanics

The investigated Dokhan volcanic (DV) rocks range in colour from green, pink and brown to purple and greyish black. The Dokhan volcanics of Um Dubr, based on field relation, could be subdivided into the following two types: a) Lower Dokhan volcanics (LDV), they crop out in the form of three elongated parallel belts of NNW-SSE trend and are conformably overlain by rocks of the upper (acidic) subdivision [42]. They are intruded by younger granites, and are

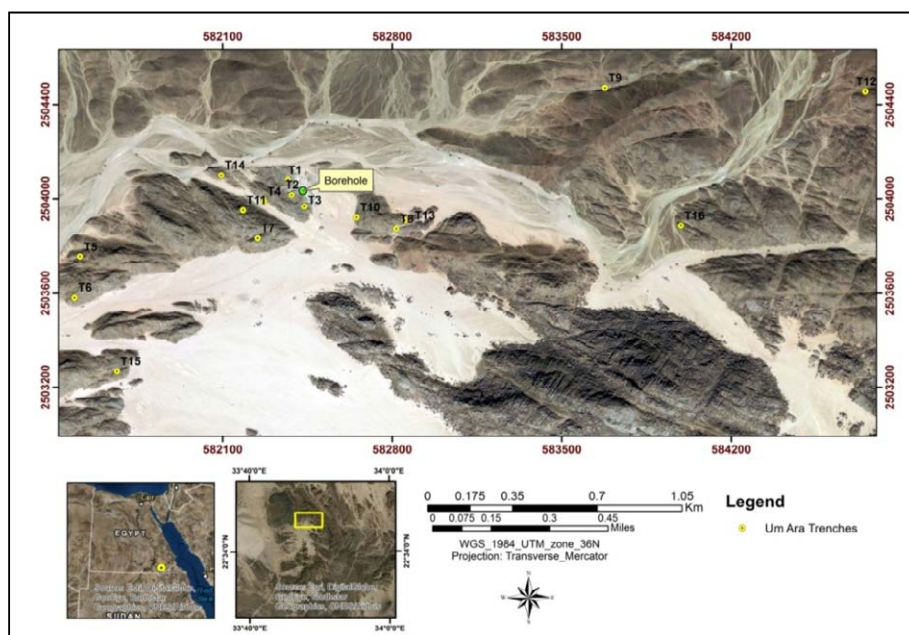


Figure 1: Location and google earth-image of the northern part of Um Ara area, South Eastern Desert (SED), Egypt.

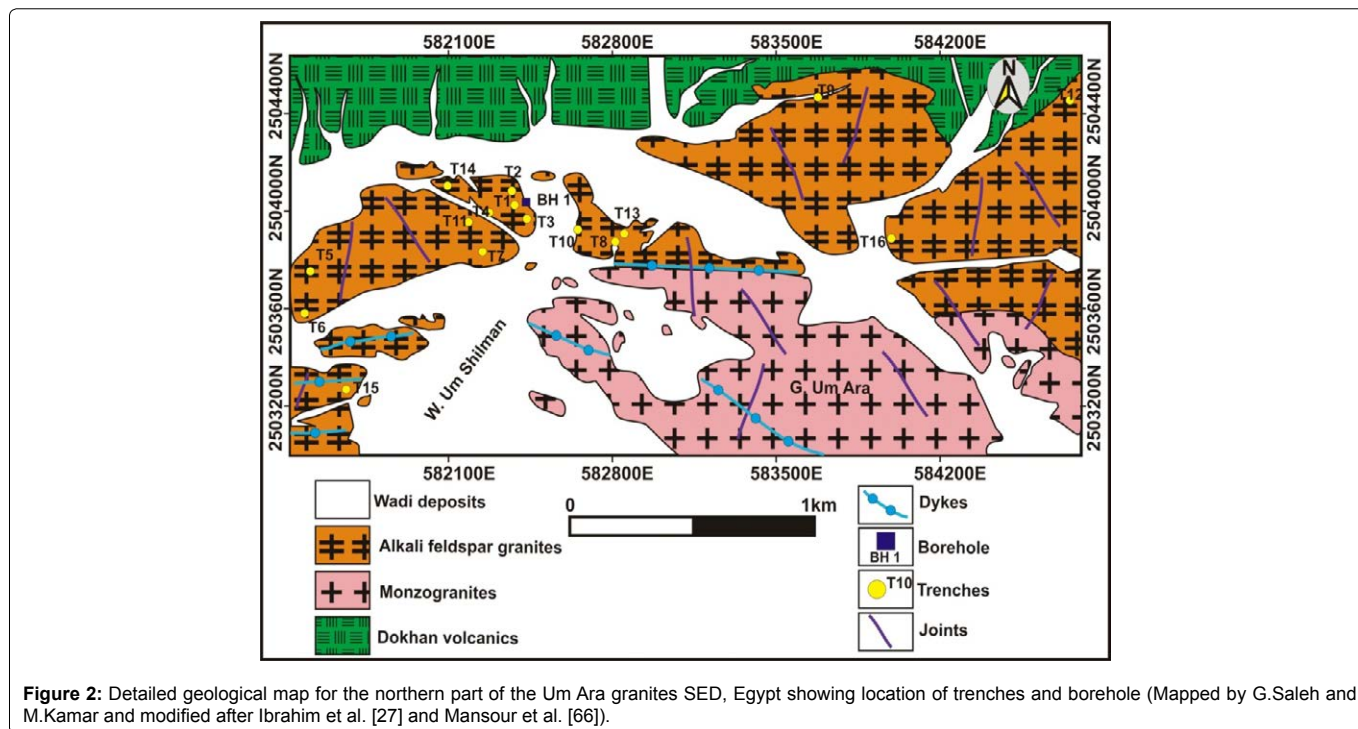


Figure 2: Detailed geological map for the northern part of the Um Ara granites SED, Egypt showing location of trenches and borehole (Mapped by G.Saleh and M.Kamar and modified after Ibrahim et al. [27] and Mansour et al. [66]).

dissected by different dyke swarms. Andesite, quartz andesite, imperial porphyry and amygdaloidal andesite and pyroclastics are recognized. b) Upper Dokhan volcanics (UDV) occur in the form of two elongated belts of NNW-SSE and N-S trends [42]. These rocks are characterized by a moderate to high topography and more felsic ones. The rocks are commonly porphyritic, massive and white to pink in colour on fresh surfaces with euhedral sulphide disseminations. Thus the upper Dokhan volcanic and their equivalents in the Eastern Desert and Sinai may represent a good target for exploration for uranium in Egypt [42].

Monzogranites

The monzogranite (coarse grained granites) is an oval-shaped pluton trending N-S to NW-SE. It is coarse-grained, massive of pale pink colour and exhibits an equigranular texture. The rock consists essentially of k-feldspar, quartz, plagioclase and biotite. Accessory minerals are opaques, apatite, titanite and zircon, while muscovite and chlorite are secondary minerals. The K-Ar age for Um Ara monzogranite is 589Ma and for the other granites 556Ma [39]. **K-feldspar** is euhedral to subhedral crystals up to 2.5mm across, in some places altered to clay and sericite. The perthite and antiperthite textures were existed. The perthitic films are arranged subparallel to each other and parallel to the cleavage planes of k-feldspar host. **Quartz** is present as large subhedral as well as fine-grained crystals occupying interstices between other constituents. It is also enclosed by both microcline and plagioclase crystals forming graphic and myrmekitic textures. **Plagioclase** is oligoclase in composition (An_{12-20}) occurs as euhedral to subhedral prisms up to 3.5mm. **Biotite** is the dominant ferromagnesian mineral in this rock type, sometimes inter-layered with chlorite. It occurs as long flakes as well as very short laths. It may contain minute inclusions of titanite, apatite, quartz and zircon (Figure 3). Opaques are present as disseminated crystals of irregular outlines or as fine aggregates in association with biotite. Muscovite has been observed in a few samples as fine alteration aggregates.

Alkali-feldspar granites

It is subsolvus, fine- to medium-grained, equigranular of light yellowish-brown to pink colour. The alkali-feldspar granites (fine grained granites) send apophyses and off shoots (ranging in thickness from 1.5 cm to 250 m) into the northern Dokhan volcanics of Gabel Um Dubr [42]. Visible secondary uranium crystals are identified in hand specimens of the alkali-feldspar granite. They occur as stains along the fracture surfaces and as acicular crystals filling cavities. The later hydrothermal activities were manifested by hematitization, albitization, K-feldspathization, chloritization, silicification with partial kaolinization together with the frequent presence of manganese oxides, green and violet fluorite and uranium mineralization (uranophane) (Figure 4).

Detailed geological map was constructed by N-S traverses. The mapping was accompanied by a systematic sampling (16 samples in trenches) at 50-100 m intervals from Um Ara mining area (Figure 2). Sixteen trenches (T) have been digged (Figure 5) in the fine grained granites to explore and investigate the alteration processes and mineralization with depth. Field observations and microscopic examinations revealed the presence of three modes of occurrence for the rare metals mineralization associated with the Um Ara granite area. These modes are: (1) disseminated mineralization of columbite, Nb-Mn-Zn rich ilmenite, Hf-rich zircon, xenotime, thorite, monazite, (2) uranium crystals and most commonly as fracture-filling and (3) minor placer occurrences of columbite, zircon, xenotime and thorite [37]. Two modes of occurrences are exhibited by the uranophane in the Um Ara granites; disseminated in the granites and fracture-fillings in the amazonitized and albitized granites. The fracture-filling uranophane is closely associated with late stage Fe and Mn oxide alteration.

Petrographically, it consists mainly of quartz, perthitic microcline with orthoclase, plagioclase of oligoclase composition, biotite and muscovite. Accessories are fluorite, garnet, titanite, apatite, and

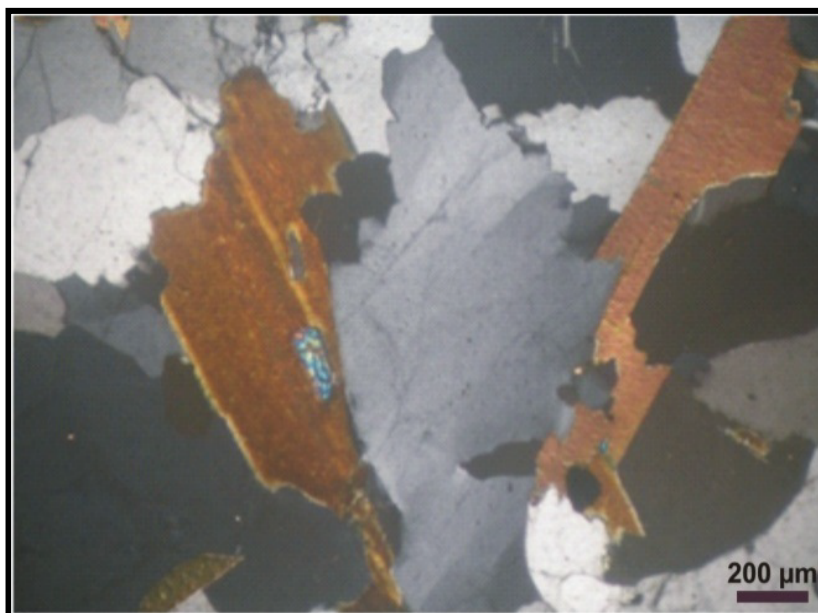


Figure 3: Photomicrograph of monzogranites showing a well-formed crystal of zircon associating with quartz and biotite, Um Ara area, SED, Egypt.

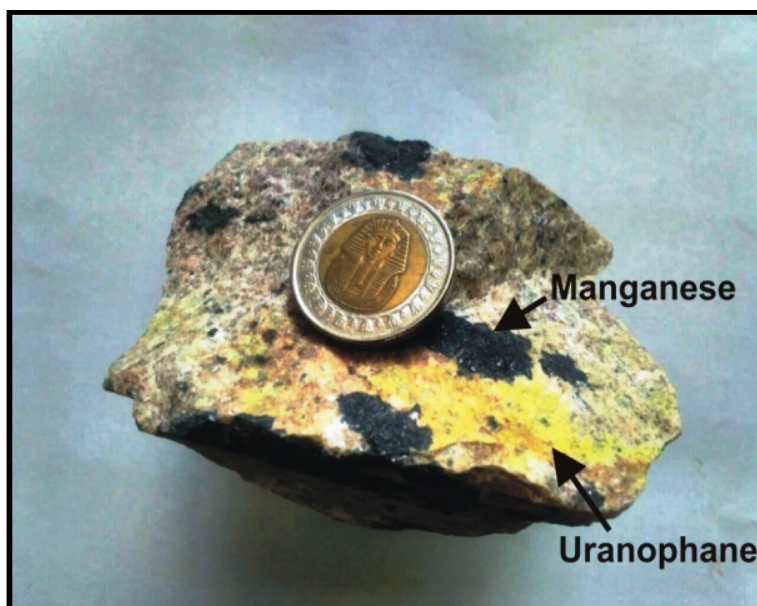


Figure 4: Visible uranium (uranophane) and manganese minerals in altered fine grained granites, Um Ara area, SED, Egypt.

opaques. **Quartz** occurs as unstrained, anhedral to subhedral grains up to 1.5mm across. Locally they form granophyric, graphic and worm-like myrmekitic intergrowths. **K-feldspar** is medium-grained up to 3.0 mm consisting of stringers and patches perthitic cross-hatched microcline with minor orthoclase (Figure 6). Some orthoclase perthite crystals exhibit simple Carlsbad twinning. **Plagioclase** crystals are medium-grained and partly saussuritized. The exsolved fine-grained plagioclase is fresh relative to the host microcline and orthoclase.

Biotite crystals are subhedral, pale reddish-brown colour and slightly altered to chlorite. **Muscovite** occurs as long prisms and small

laths, and as inclusions in plagioclase with preferred orientation. Corroded boundaries of muscovite are common as well as wavy extinction.

Fluorite crystals are intergranular to orthoclase perthite indicating their late crystallization. Euhedral crystals of **garnet** are present through some samples of the alkali feldspar granite. Opaque minerals occur as subhedral grains as well as irregular granules mostly enclosed by biotite. **Titanite** occurs either as well developed small crystals always associated with the biotite or as thin rims around titaniferous opaques. **Apatite** occurs as short prisms or minute needles or six-sided grains enclosed in plagioclase feldspar and biotite. The presence

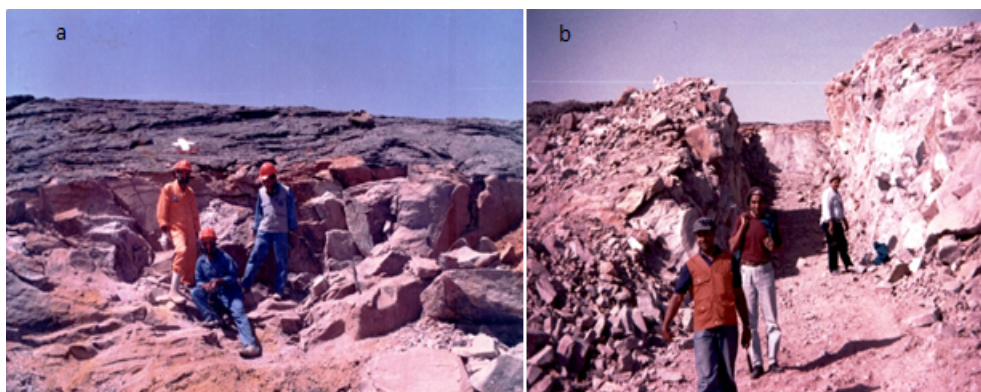


Figure 5: View showing (a) the initiation of drilling trench (Photo by G.M.Saleh) and (b) after completing drilling of trench No.1 Um Ara area (Mansour et al. [66], Photo by G.M.Saleh), SED, Egypt, looking W.

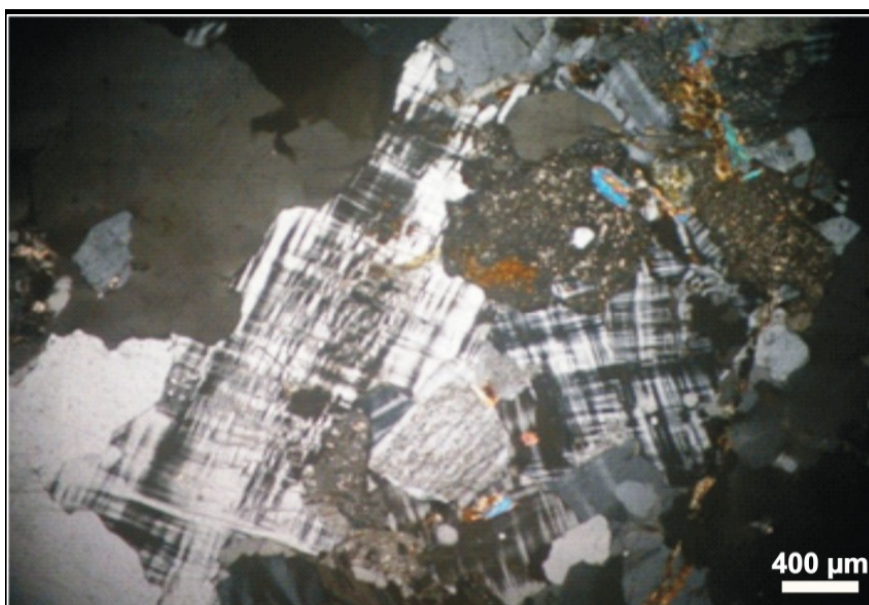


Figure 6: Photomicrograph of alkali feldspar granites showing plagioclase partially transformed to microcline (microclinization), Um Ara area, SED, Egypt.

of leached biotite, hematite and fluorite clots in the alkali feldspar granite indicates the role of fluid- and fluorine-rich volatile activity.

Geochemistry

Analytical methods

Sixteen (16) and ten (10) samples were collected representing the altered granites and core samples respectively. The collected samples were chemically analyzed using different analytical procedures at the laboratories of the Nuclear Materials Authority of Egypt (NMA). Precision of the analytical data was monitored by international rock standards and is better than 3% for major oxides and 5% for trace elements. The REEs were analyzed using an ICP-AES spectrometer. Loss on ignition (LOI) was calculated by heating about 3g of a rock powder in a porcelain crucible at about 1000°C for 4 hours. The results of the chemical analyses are given in Tables 1 to 4. All samples represent north Um Ara granitic rocks (alkali feldspar granites) and each sample is represented by the location (number of trench and its

UTM) and chemical value (ppm).

Geochemical characteristics

There are a variation in trace elements and rare earth elements (REEs) concentrations in both trenches and core samples as follows: The average concentration of Cu, Zn, Zr, Rb, Y, Pb, Ga, Nb and all rare earth elements except Gd and Tm in core samples are higher than that in trenches, while the concentration of Ba, Sr, U, Th, Gd and Tm in trenches are higher than that in core samples (Figures 7,8).

According to Meyer et al. [43], Um Ara granites trenches and core samples are plotting on AKF ternary diagram (Figure 9), where $A = Al_2O_3 - (Na_2O + K_2O)$, $K = K_2O$ and $F = FeO + MnO + MgO$. It shows that only four samples of the altered granites from trenches fall alteration fields, two of them fall in sericite facies (due to sericitization processes) and the other two samples fall in propylitic field. All the core samples fall out of alteration fields.

The weathering trends are displayed on $(Na_2O + CaO) - Al_2O_3 - K_2O$ triangular diagram (Figure 10) [44,45], Um Ara granites

Table 1: Chemical composition of major oxides (Wt%) and trace elements (ppm) analyses of uraniferous granitic rocks of the trenches samples, Um Ara area, SED, Egypt.

Sample no	T1	T2	T3	T4	T5	T6	T7	T8	T9	T10	T11	T12	T13	T14	T15	T16
SiO ₂	72.62	75.74	75.13	71.99	73.09	75.28	74.35	73.95	73.51	74.65	74.52	74.79	75.19	74.39	74.96	73.34
TiO ₂	0.01	0.02	0.03	0.01	0.51	0.42	0.08	0.02	0.12	0.11	0.13	0.35	0.09	0.14	0.29	0.22
Al ₂ O ₃	13.13	12.02	12.25	13.07	12.45	11.99	13.12	14.16	14.26	13.96	13.86	12.52	13.59	13.51	12.67	13.48
Fe ₂ O ₃	1.75	1.87	1.79	1.72	2.55	1.42	1.94	1.82	1.87	0.93	1.98	2.32	1.64	0.97	1.62	1.49
MnO	0.03	0.01	0.02	0.05	0.21	0.12	0.11	0.16	0.03	0.02	0.03	0.24	0.04	0.06	0.13	0.05
MgO	0.04	0.03	0.05	0.09	0.19	0.14	0.12	0.09	0.08	0.07	0.12	0.09	0.06	0.08	0.12	0.19
CaO	0.89	0.24	0.45	0.8	0.62	0.35	0.49	0.39	0.2	0.12	0.28	0.41	0.24	0.34	0.54	0.85
Na ₂ O	3.86	3.79	4.52	4.59	4.42	3.79	3.12	4.38	3.45	3.88	3.72	3.59	3.71	3.71	3.71	3.48
K ₂ O	6.61	5.85	5.36	7.45	4.71	4.96	5.24	3.72	5.47	5.51	4.52	4.76	4.77	5.69	4.82	4.98
P ₂ O ₅	0.02	0.01	0.02	0.01	0.11	0.13	0.18	0.21	0.04	0.03	0.02	0.02	0.03	0.04	0.05	0.04
L.O.I	0.45	0.19	0.22	0.18	0.61	0.92	0.75	0.65	0.59	0.62	0.35	0.81	0.29	0.56	0.73	1.63
Total	99.41	99.77	99.84	99.96	99.47	99.52	99.5	99.55	99.62	99.9	99.53	99.9	99.65	99.49	99.64	99.75
Trace Elements																
Cu	35	69	44	57	25	17	22	18	69	37	14	55	78	35	14	82
Zn	252	156	234	112	77	65	165	197	109	145	76	156	89	109	95	175
Zr	307	279	385	292	143	98	182	125	322	275	243	214	227	157	233	195
Rb	539	442	793	554	79	68	465	632	219	316	306	98	332	415	79	85
Y	117	135	145	95	59	72	66	59	82	116	85	83	122	113	49	65
Ba	66	115	95	75	266	293	121	81	57	64	72	129	134	91	175	272
Pb	88	139	192	272	25	37	52	98	69	48	47	29	62	102	33	58
Sr	42	35	28	45	76	32	29	32	45	49	65	44	37	63	47	26
Ga	72	84	43	69	56	37	58	62	39	42	52	32	65	52	38	43
Nb	112	273	226	253	175	65	74	156	96	115	97	88	66	127	96	109
U	433	506	307	255	196	175	214	197	185	272	278	185	155	225	195	154
Th	58	59	110	65	47	54	79	372	298	415	82	329	275	82	67	255

Table 2: REEs concentration in trenches at Um Ara area, SED, Egypt.

Elements	T1	T2	T3	T4	T5	T6	T7	T8	T9	T10	T11	T12	T13	T14	T15	T16
La	75.68	83.15	52.49	76.08	36.02	47.85	52.31	51.58	29.51	41.43	35.71	75.82	47.55	33.59	25.15	40.66
Ce	91.49	132.92	124.12	66.75	130.08	89.1	45.55	61.78	53.16	81.15	49.52	110.12	31.12	48.63	59.13	70.19
Pr	5.45	9.82	8.23	7.47	4.29	7.09	4.55	3.64	3.88	9.18	7.49	10.15	8.15	6.88	5.09	6.16
Nd	48.77	65.16	46.29	38.75	63.39	40.12	11.36	10.22	27.72	38.09	13.25	70.36	17.16	24.36	26.12	30.12
Sm	4.22	7.36	4.81	5.15	2.16	3.14	2.19	3.89	5.63	6.55	2.59	5.96	4.49	5.61	4.97	6.12
Eu	0.33	0.73	0.24	0.19	0.39	0.22	0.32	0.28	0.42	0.72	0.48	0.79	0.47	0.53	0.69	0.83
Gd	1.18	1.84	1.85	1.77	0.59	0.49	1.45	1.96	1.45	1.31	1.51	2.69	6.09	5.82	4.1	5.12
Tb	0.48	1.39	0.32	1.62	1.76	0.96	1.49	0.89	0.97	0.12	0.57	1.96	0.85	0.71	0.79	0.92
Dy	1.75	1.09	1.24	1.02	0.96	0.67	1.12	3.55	1.11	1.73	2.22	0.66	0.46	1.89	0.7	1.89
Ho	1.07	0.58	1.29	1.61	0.77	0.86	0.69	0.57	1.31	0.77	0.79	1.43	1.29	1.35	0.86	0.7
Er	0.89	0.92	0.86	1.19	0.73	0.79	1.28	1.11	0.62	1.22	0.88	1.39	0.13	1.28	0.45	0.76
Tm	0.86	0.82	0.91	1.07	0.73	0.49	0.29	0.23	0.55	0.77	0.36	0.42	0.57	0.62	0.61	0.73
Yb	1.88	1.69	1.15	1.62	0.39	0.46	1.35	1.12	0.29	0.21	1.45	1.36	0.48	1.32	1.43	1.25
Lu	0.37	0.81	0.75	0.92	0.78	0.54	0.75	0.43	0.38	0.65	0.59	0.52	0.52	0.49	0.21	0.39
REEs	234.42	308.28	244.55	205.21	243.04	192.78	124.7	141.25	127	183.9	117.41	283.63	119.33	133.08	130.3	165.84
LREEs	225.61	298.41	235.94	194.2	235.94	187.3	115.96	131.11	119.9	176.4	108.56	272.41	108.47	119.07	120.46	153.25
HREEs	8.81	9.87	8.61	11.01	7.1	5.48	8.74	10.14	7.1	7.5	8.85	11.22	10.86	14.01	9.84	12.59
L/H	25.61	30.23	27.4	17.64	33.23	34.18	13.27	12.93	16.89	23.52	12.27	24.28	9.99	8.5	12.24	12.17
(Eu/Eu*)_n	0.45	0.61	0.25	0.19	1.06	0.54	0.55	0.31	0.45	0.75	0.74	0.6	0.27	0.28	0.47	0.45
t₁	0.5	0.67	0.89	0.56	0.68	0.79	0.81	0.9	0.69	0.94	1.22	0.63	0.77	0.88	0.93	0.82
t₃	0.9	1.32	0.45	0.84	2.13	1.36	1.43	1.86	0.83	0.5	1.14	0.64	0.25	0.46	0.44	0.77
t_{1,3}	0.67	0.94	0.63	0.69	1.2	1.04	1.08	1.29	0.76	0.69	1.18	0.63	0.43	0.63	0.64	0.79

Normalized REEs after Boynton [65]. $Eu/Eu^* = EuN / ((SmN) \cdot (GdN))^{0.5}$ according to Taylor et al. [55].

trenches and core samples show a relative enrichment in K₂O and Al₂O₃ compositions due to the relative alteration of feldspars to clay minerals.

The Na-K variations diagram after Cuney et al. [46] shows

five trends; Na-metasomatism, K-metasomatism, silicification, desilicification and argillation (Figure 11). Most of Um Ara granites trenches and core samples lie in K-metasomatism trend.

The most prominent geochemical characteristics of Um Ara

Table 3: Chemical composition of major oxides (Wt%) and trace elements (ppm) analyses of uraniferous granitic rocks of the core samples, Um Ara area, SED, Egypt.

Sample no/ Depth	C1 (10m)	C2 (20m)	C3 (40m)	C4 (60m)	C5 (80m)	C6 (100m)	C7 (115m)	C8 (130m)	C9 (145m)	C10 (165m)
SiO ₂	73.78	74.37	74.39	75.51	73.65	73.83	74.47	75.37	73.56	74.66
TiO ₂	0.09	0.05	0.11	0.07	0.04	0.02	0.05	0.02	0.05	0.07
Al ₂ O ₃	13.88	13.72	14.32	13.17	14.35	14.21	13.52	13.62	14.32	13.39
Fe ₂ O ₃	0.95	1.42	0.73	0.95	1.09	0.82	0.99	0.58	1.27	0.83
MnO	0.18	0.45	0.39	0.26	0.14	0.13	0.19	0.14	0.19	0.21
MgO	0.11	0.14	0.17	0.23	0.19	0.14	0.21	0.15	0.13	0.19
CaO	0.29	0.36	0.29	0.19	0.33	0.21	0.16	0.22	0.14	0.25
Na ₂ O	3.24	3.35	3.19	3.51	3.74	3.62	4.09	4.15	3.72	4.25
K ₂ O	6.15	5.76	5.55	6.27	5.36	5.84	5.42	5.26	6.67	5.18
P ₂ O ₅	0.05	0.07	0.05	0.03	0.09	0.11	0.08	0.08	0.05	0.07
L.O.I	0.85	0.78	0.95	0.84	0.92	0.66	0.59	0.69	0.73	0.82
Total	99.57	100.47	100.14	100.67	99.9	99.59	99.77	100.28	100.83	99.92
Trace Elements										
Cu	42	75	56	49	35	46	69	82	95	77
Zn	254	165	132	275	145	176	224	199	159	214
Zr	148	254	175	149	285	292	172	385	279	257
Rb	420	329	498	369	511	452	335	556	281	423
Y	107	65	94	88	101	79	68	114	120	99
Ba	114	66	72	15	59	62	55	83	115	111
Pb	89	105	121	69	94	116	146	168	153	172
Sr	21	33	25	32	15	14	22	19	39	42
Ga	62	51	77	102	98	36	85	67	115	121
Nb	175	162	86	185	89	189	277	182	297	179
U	128	159	218	349	265	179	212	255	296	312
Th	45	69	105	146	123	89	109	122	135	131

Table 4: REEs concentration in core samples at Um Ara area, SED, Egypt.

Elements /Depth	C1 (10m)	C2 (20m)	C3 (40m)	C4 (60m)	C5 (80m)	C6 (100m)	C7 (125m)	C8 (130m)	C9 (145m)	C10 (165m)
La	89.15	133.75	159.73	75.85	69.14	56.21	86.12	41.19	126.12	112.15
Ce	115.12	128.12	101.86	95.77	99.65	86.15	78.11	95.19	119.15	127.12
Pr	35.13	19.16	23.62	45.27	49.66	38.17	27.19	35.56	48.62	28.25
Nd	69.15	72.16	49.56	52.97	43.79	38.17	41.15	53.69	75.12	78.69
Sm	17.12	14.27	9.79	13.92	12.11	18.14	13.49	16.75	15.77	12.15
Eu	0.28	0.79	0.86	0.59	0.45	0.32	0.46	0.49	0.28	0.89
Gd	3.66	1.26	2.12	3.39	1.24	2.11	1.73	3.45	1.96	3.22
Tb	2.19	1.66	1.34	1.74	1.46	1.29	1.44	1.67	1.88	1.19
Dy	2.26	3.42	4.52	3.12	3.97	5.21	2.95	4.19	3.39	1.99
Ho	1.51	1.44	1.27	2.15	1.42	1.31	1.29	1.35	1.21	1.15
Er	2.63	3.23	1.62	3.29	2.11	4.29	2.19	3.59	1.38	3.15
Tm	0.82	0.59	0.48	0.86	0.55	0.67	0.49	0.57	0.39	0.42
Yb	2.13	1.19	3.42	2.19	3.82	3.72	2.96	3.19	1.27	2.95
Lu	0.79	0.63	0.78	0.51	0.77	0.75	0.48	0.59	0.68	0.52
REEs	341.94	381.67	360.97	301.62	290.14	256.51	260.05	261.47	397.22	373.84
LREEs	325.67	367.46	344.56	283.78	274.35	236.84	246.06	242.38	384.78	358.36
HREEs	16.27	14.21	16.41	17.84	15.79	19.67	13.99	19.09	12.44	15.48
L/H	20.02	25.86	21	15.91	17.37	12.04	17.59	12.70	30.93	23.15
(Eu/Eu)ⁿ	0.11	0.57	0.58	0.26	0.36	0.16	0.29	0.2	0.15	0.44
t1	1.11	0.69	0.76	1.43	1.76	1.70	1.06	1.70	1.07	0.88
t3	1.04	1.95	1.66	0.95	2.00	1.72	1.52	1.35	1.81	0.88
t1,3	1.08	1.16	1.12	1.17	1.88	1.71	1.27	1.52	1.39	0.88

Normalized REEs after Boynton [66]. $Eu/Eu^n = EuN / [(SmN) \cdot (GdN)]^{0.5}$ according to Taylor et al. [52].

granites trenches and core samples include substantial variations in the concentrations of Na, Ca, Mg and Fe (Figure 12) [47]. Increasing alteration intensity is coupled with a gradual decrease in Na₂O and CaO, culminating in intensely altered samples having Na₂O+CaO values wt%. This trend is indicative of plagioclase destruction and

formation of muscovite/sericitization.

The alteration box plot is a graphical representation that uses two alteration indices: the Ishikawa alteration index (AI) = $100 (K_2O + MgO) / (K_2O + MgO + Na_2O + CaO)$ and the chlorite carbonate

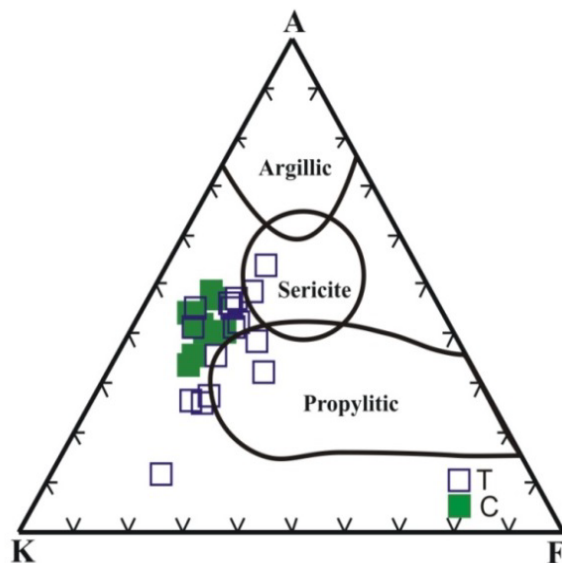


Figure 9: AKF ternary diagram for Um Ara granites trenches (T) and core (C) samples, after Meyer et al. [43], A= $Al_2O_3 - (Na_2O + K_2O)$, K= K_2O and F= $FeO+MnO+MgO$.

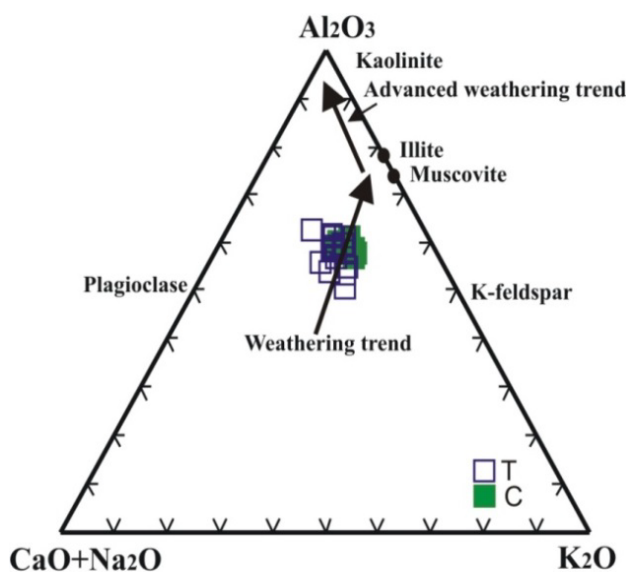


Figure 10: $Al_2O_3-(CaO + Na_2O) - (K_2O)$ ternary diagram for Um Ara granites trenches (T) and core (C) samples, after Nesbitt et al. [44,45].

core samples shows less Th/U ratio (Figure 14) than that of the crustal value [55]. All the granite samples from Um Ara granites trenches and core samples plot along the U and Th and away from the K which implies the deficiency of K and enrichment of U and Th (Figure 15).

There are two groups of trenches samples, the first one richer in Th than U, therefore they plotted between lines $U/Th=0.5$ and 1. The second group is richer in U than Th, therefore they plotted under the line of $U/Th=2$ (Figure 16). All the core samples are richer in U than Th, so they lie under the line $U/Th=2$ (Figure 16). All Um Ara granites trenches and core samples define hydrothermal U enrichment trend.

The lowest concentration of uranium and thorium in core samples

is at 10m depth, while the highest values at 60m depth (Figure 17).

The Um Ara granites trenches and core samples have variable total REEs contents 117.41 to 308.28 and 256.51 to 397.22 ppm respectively (Table 2, Table 4). $\Sigma LREEs$ in trenches and core samples range from 108.47 to 298.41 ppm and from 236.84 to 384.78 ppm respectively, whereas $\Sigma HREEs$ range from 5.48 to 14.01 ppm and from 12.44 to 19.67 ppm respectively. The lowest concentration of total REEs in core samples is at 100m depth, while the highest values at 145m depth (Figure 18).

The Chondrite-normalized REEs patterns (Figure 19), of Um Ara granites trenches and core samples are characterized by strong ($\Sigma LREEs$)n enrichment and low ($\Sigma HREEs$)n content due to the

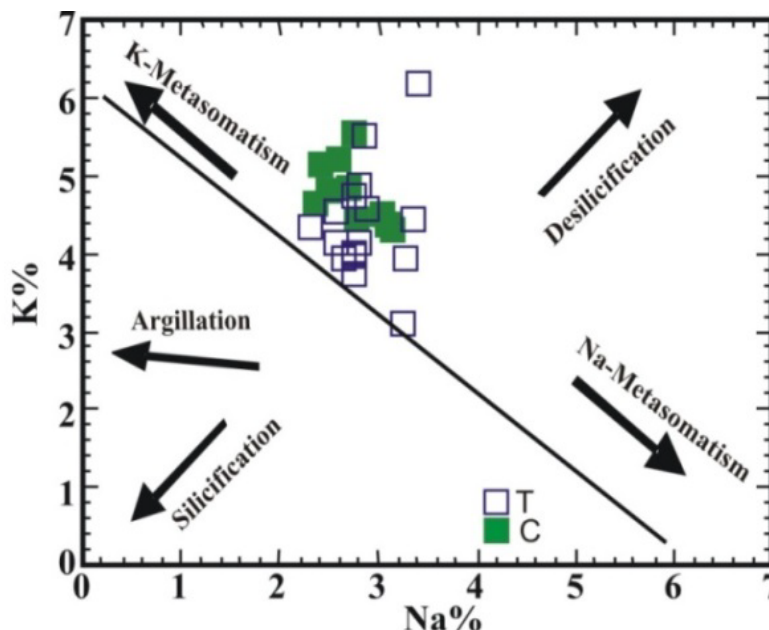


Figure 11: Na% - K% variation diagram for Um Ara granites trenches (T) and core (C) samples, showing the alteration type, after Cuney et al. [46].

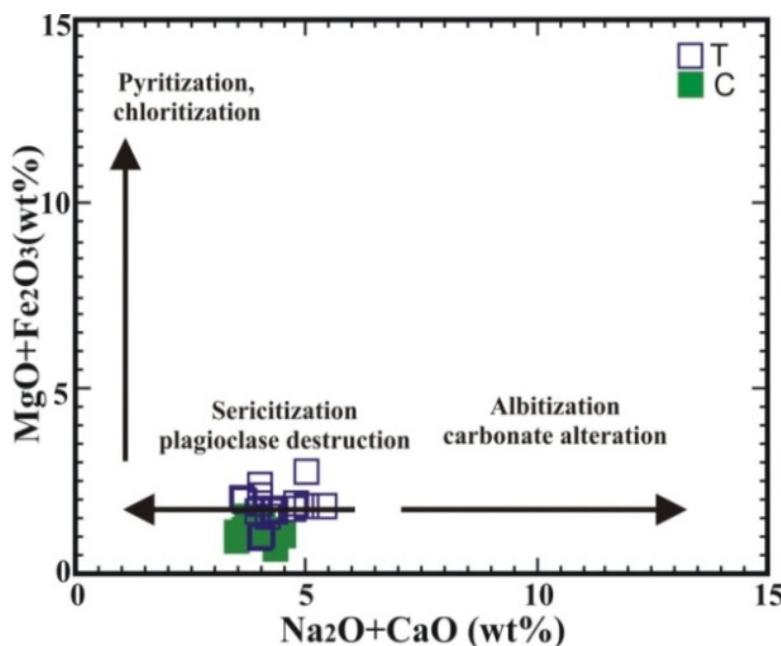


Figure 12: Alteration factors for Um Ara granites trenches (T) and core (C) samples.

presence of some accessory minerals like apatite, and zircon. The $(Eu/Eu^*)_n$ in Um Ara granites trenches and core samples ranges from 0.19 to 1.06 and from 0.11 to 0.58 respectively suggests that plagioclase was an early fractionating phase.

The tetrad effect has been progressively recognized particularly for the granitic rocks which have undergone a high degree of fractional crystallization, hydrothermal alteration, and mineralization [58-62]. Masuda et al. [41] classified the tetrad effects into two different types, M and W-type (M-type in solid sample as residues and W-type in the

interacting fluids as extract). The tetrad effect in the studied Um Ara granites trenches and core samples were calculated according to Irber equations [61]:

$$t_1 = (Ce/Ce^t \times Pr/Pr^t)^{0.5}, t_3 = (Tb/Tb^t \times Dy/Dy^t)^{0.5} \text{ and } T_{1,3} = (t_1 \times t_3)^{0.5}$$

When $TE_{1,3}$ values are higher than 1.1, the rock is considered to show the tetrad effect. The studied Um Ara granites trenches have $TE_{1,3}$ values range from 0.43 to 1.29, so they do not show tetrad effect in most samples (Table 2), whereas in core samples $TE_{1,3}$ value ranges

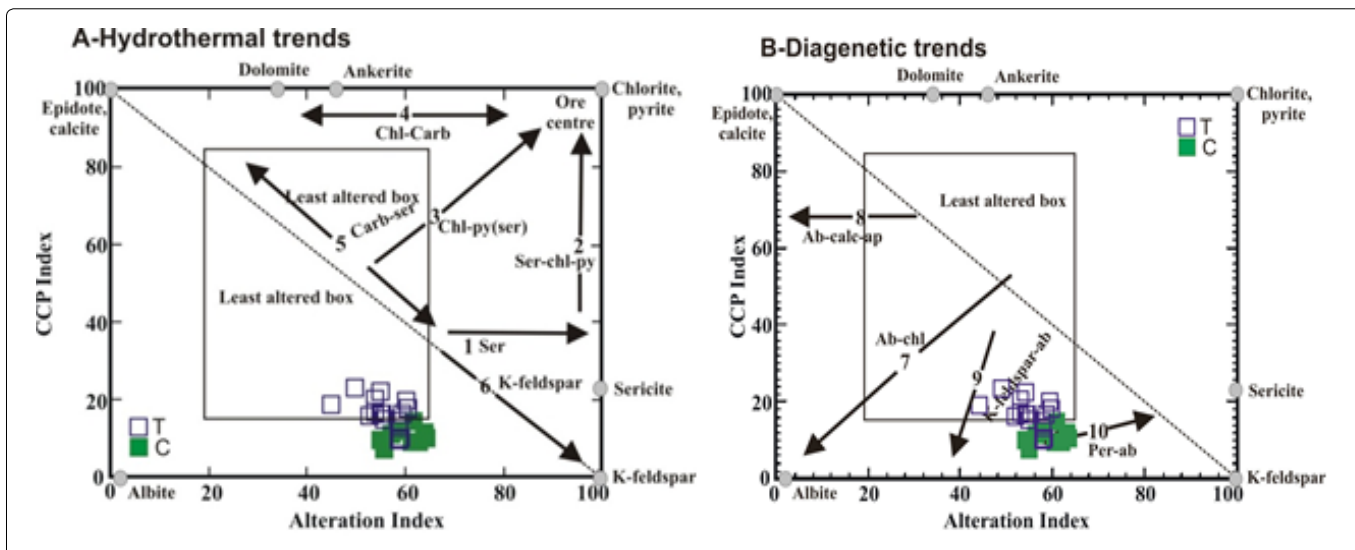


Figure 13: A hydrothermal and diagenetic alteration box plot diagram for Um Ara granites trenches (T) and core (C) samples, (after Large et al. [48]). The trend No. 9 (after Gifkins et al. [54]).

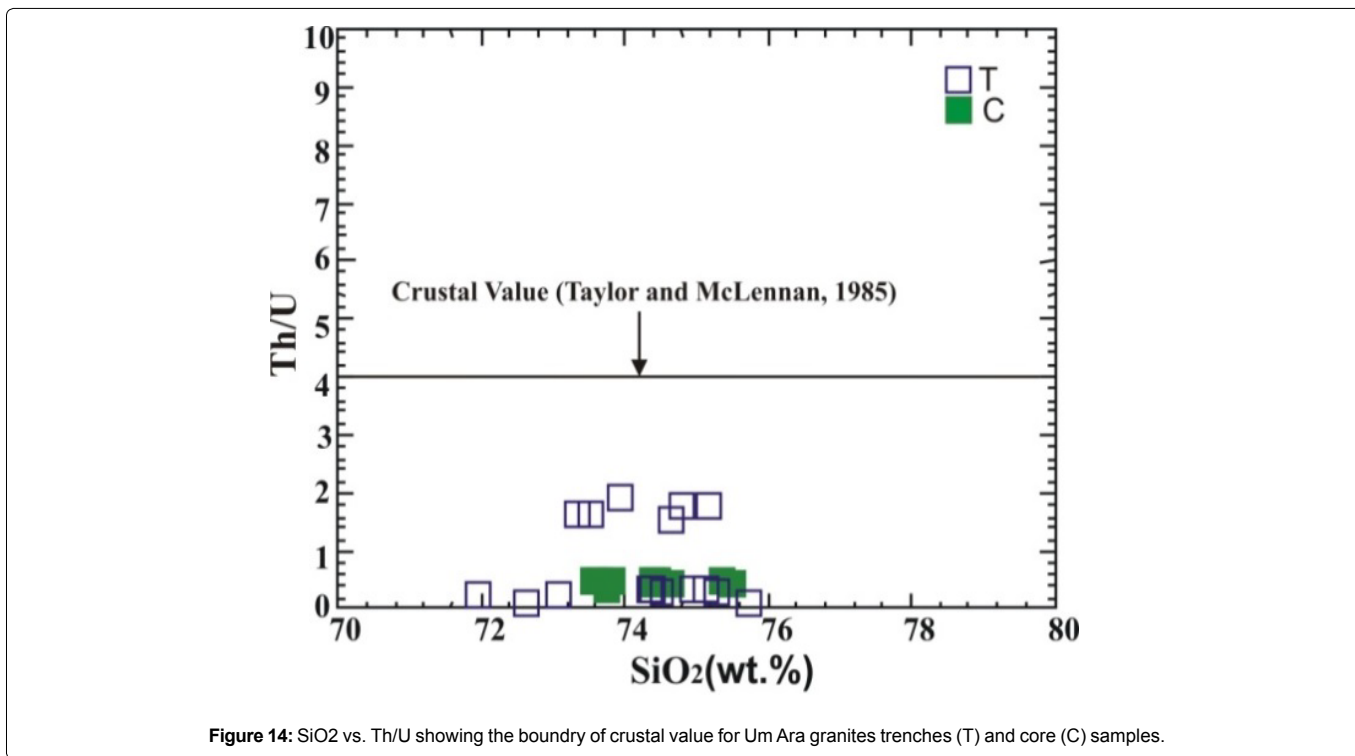


Figure 14: SiO₂ vs. Th/U showing the boundry of crustal value for Um Ara granites trenches (T) and core (C) samples.

from 0.88 to 1.88 showing tetrad effect. The fractionation of elements with similar ionic radius and charge is regarded to be sensitive to change in the melt composition during magma differentiation [60,63].

The geochemical data suggest that the Um Ara granites trenches and core samples has evolved by means of fractional crystallization through removal of K-feldspar, biotite, plagioclase, together with some accessories such as apatite and Fe-Ti oxide phases. From the HREE pattern, the elements (Tb, Ho, Tm and Lu) form positive anomaly rather than (Dy, Er and Yb) in some samples of Um Ara granites trenches and core samples it may be suggested that fluorine-

complexes played some role during its evolution.

Mineralogical features

The heavy minerals were separated using heavy liquid (bromoform) separation technique, followed by magnetic fractionation using Frantz isodynamic separator. The heavy minerals were picked under a binocular microscope and identified by Environmental Scanning Electron Microscope (ESEM) techniques. All analyses have been done at Nuclear Materials Authority (NMA), Cairo, Egypt.

The altered granites contain uranium, thorium minerals,

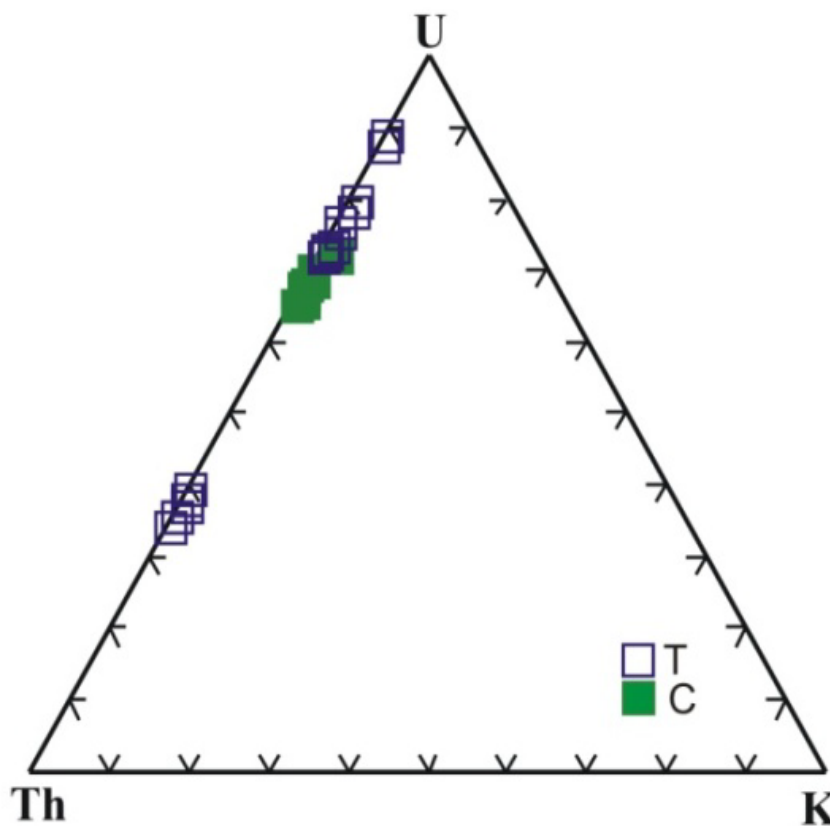


Figure 15: K-U-Th diagram showing the concentration of K, U, Th for Um Ara granites trenches (T) and core (C) samples.

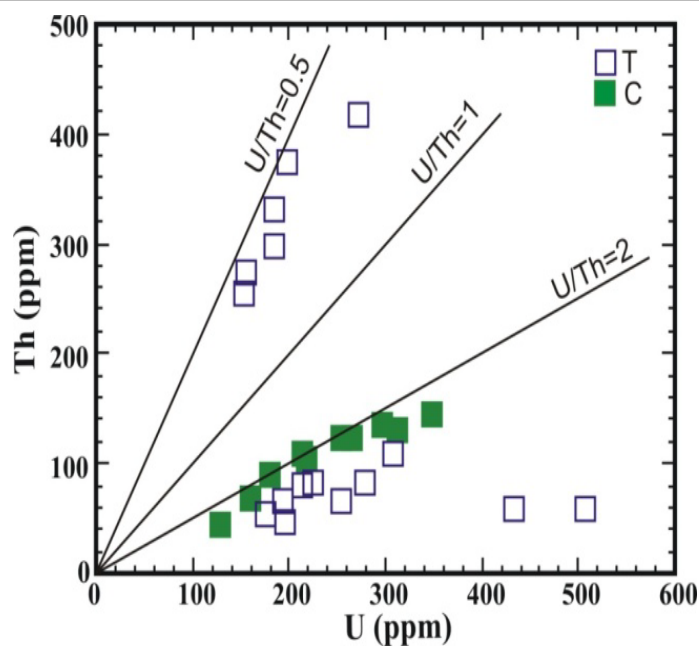


Figure 16: U-Th relationships for Um Ara granites trenches (T) and core (C) samples.

uranium bearing minerals and Nb-Ta mineral. The uranium mineral is uranophane (Figure 20) and thorium mineral is uranothorite. The

uranium bearing minerals are fluorite, monazite, xenotime, allanite, zircon while Nb-Ta mineral is columbite (Figure 21).

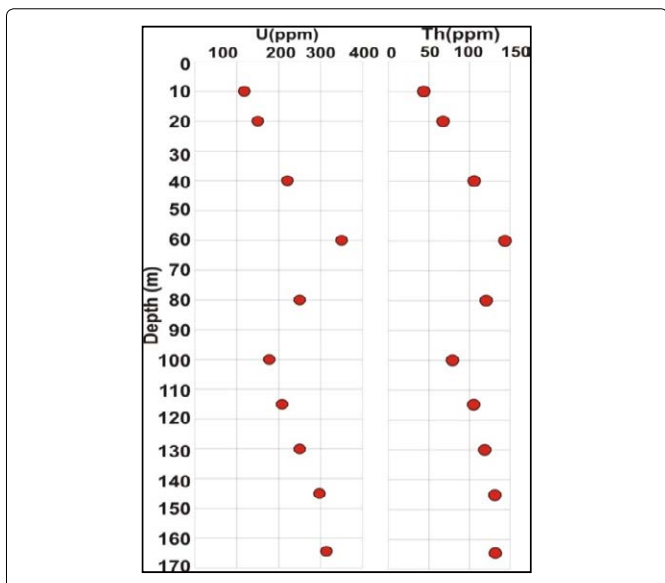


Figure 17: Downhole variation in U and Th (ppm) of Um Ara granites core samples.

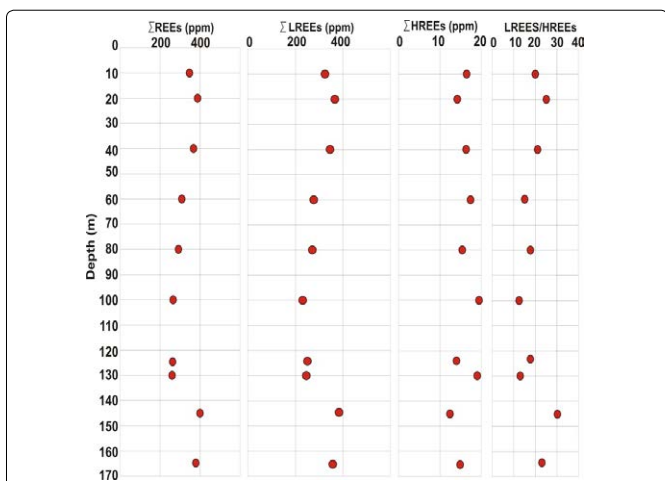


Figure 18: Downhole variation in REE, LREE, HREE, and LREE/HREE of Um Ara granites core samples.

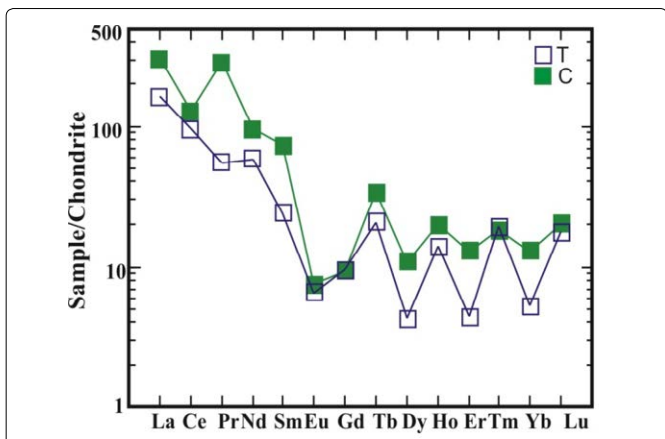


Figure 19: Chondrite-normalized REE patterns for Um Ara granites trenches (T) and core (C) samples, Normalizing values (after Boynton et al. [65]).

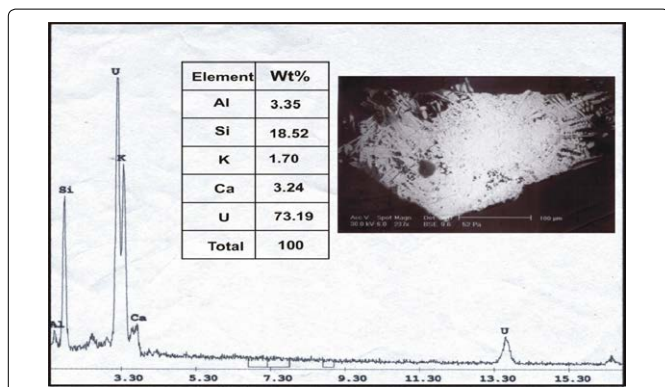


Figure 20: ESEM back-scattered data and image of uranophane, Um Ara area, SED, Egypt.

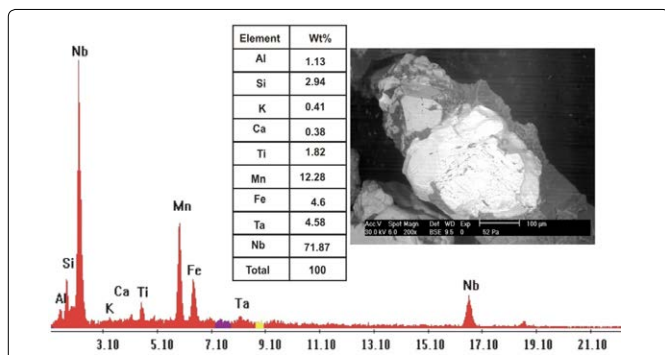


Figure 21: ESEM back-scattered data and image of columbite, Um Ara area, SED, Egypt.

Uranium and thorium estimation from trenches excavations

The estimation of uranium and thorium depend on the samples taken from the trenches and calculated as follows:

$$\text{Total samples} = \text{Total collected samples.}$$

$$\text{Av. element content (ppm)} = \frac{\text{Total element content}}{\text{No. of selected samples.}}$$

$$\text{Element grade (\%)} = \frac{\text{Av. element content}}{10000}.$$

$$\text{Volume (m}^3\text{)} = \text{Length} \times \text{width} \times \text{depth of selected area.}$$

$$\text{Element tonnage (t)} = \text{Volume} \times 2.60 \text{ (average density of granites)}$$

$$\text{Element metal (t)} = \text{Element tonnage} \times \text{element grade.}$$

The average of uranium and thorium mineralization grade and the total tonnage in all trenches are calculated as illustrated in table 5 and that of the total trenches are calculated in Table 6.

Conclusion

The following are the main detailed geological, petrological and geochemical works, and previous results revealed the following characteristics for Um Ara area:

The basement rock units of Um Ara area is a part of the Arabian-Nubian Shield between 581400m E-584900m E and 2503000m N-2504600m N. They are represented by Dokhan volcanic and post-collision granitoids (monzogranite, and alkali feldspar granite), dykes and quartz veins. It could be concluded that the major NNW-SSE, NNE-SSW and NE-SW trending fracture sets were acted as the principal channel ways for the mineralized solution while the re-

Table 5: Illustrating the tonnage (ton), element grade (%) and element metal (ton) for uranium and thorium mineralization in Um Ara granites trenches area, SED, Egypt.

Trenches	T1		T2		T3		T4	
Elements	U	Th	U	Th	U	Th	U	Th
Volume (m ³)	372m ³		918 m ³		918 m ³		270 m ³	
Tonnage (ton)	967.2 ton		2386.8 ton		2386.8 ton		702 ton	
Element grade (%)	0.0433	0.0058	0.0506	0.0059	0.0307	0.011	0.0255	0.0065
Element metal (ton)	0.419	0.056	1.21	0.141	0.733	0.263	0.179	0.046
Trenches	T5		T6		T7		T8	
Elements	U	Th	U	Th	U	Th	U	Th
Volume (m ³)	315 m ³		144 m ³		141.75 m ³		81 m ³	
Tonnage (ton)	819 ton		374.4 ton		368.55 ton		210.6 ton	
Element grade (%)	0.0196	0.0047	0.0175	0.0054	0.0214	0.0079	0.0197	0.0372
Element metal (ton)	0.161	0.038	0.066	0.02	0.079	0.029	0.041	0.078
Trenches	T9		T10		T11		T12	
Elements	U	Th	U	Th	U	Th	U	Th
Volume (m ³)	81 m ³		20.25 m ³		31.5 m ³		72 m ³	
Tonnage (ton)	210.6 ton		52.65 ton		81.9 ton		187.2 ton	
Element grade (%)	0.0185	0.0298	0.0272	0.0415	0.0278	0.0082	0.0185	0.0329
Element metal (ton)	0.039	0.063	0.014	0.022	0.023	0.007	0.035	0.062
Trenches	T13		T14		T15		T16	
Elements	U	Th	U	Th	U	Th	U	Th
Volume (m ³)	132 m ³		120 m ³		52.5 m ³		52.5 m ³	
Tonnage (ton)	343.2 ton		312 ton		136.5 ton		136.5 ton	
Element grade (%)	0.0155	0.0275	0.0225	0.0082	0.0195	0.0067	0.0154	0.0255
Element metal (ton)	0.053	0.094	0.07	0.026	0.027	0.009	0.021	0.035

Table 6: Illustrating the tonnage (ton), element grade (%) and element metal (ton) for uranium and thorium mineralization in the all Um Ara granites trenches, SED, Egypt.

Elements	U	Th
Volume (m ³)	3721.5 m ³	
Tonnage (ton)	9675.9 ton	
Element grade (%)	0.0246	0.01654
Element metal (ton)	2.38 ton	1.6 ton

deposition took place within almost all the minor fracture trends with no preferred orientation.

Um Ara altered granites and core samples are considered to be low grade uranium mineralization. This area seems to have been affected by many groundwater activities. The origin of the secondary uranium minerals is mainly related to alteration of primary uranium minerals by the action of oxidizing fluid (supergene alteration) mobilization of uranium and then re-deposition in other forms. Redistribution by circulating meteoric waters might have taken place. The rocks are characterized by containing of mineralization as uranium mineral (uranophane), thorium mineral (uranthorite) and others minerals such as (columbite, fluorite, monazite, xenotime, allanite and zircon).

Highest uranium concentrations, that are associated with altered trench granites and core samples rocks, show strongest broad uranium anomaly, with irregular shape. The radioactivity was measured systematically in the field over a grid with 0.5 meter spacing, constructed in the trenches. The rocks and their alteration products are the main constituents of these trenches. Hematization is mostly present as well as other different types of alterations such as sericitization, albitization, K-feldspathization, chloritization, silicification, argillization, fluoritization, kaolinitization and limonitization. These alterations are concentrated along the

fractures of altered granite and are associated with mineralization.

Um Ara altered granites trenches are an abnormal radiation and have an extension. So, these anomalies are suitable to be a place for uranium extraction. The preliminary estimation of average element grade (%) of uranium and thorium mineralization in trenches is: U (0.0246%) and Th (0.01654%). The preliminary estimation of average element metal (by tons) of radioactive elements in trenches: U (2.38) and Th (1.6). Preliminary results show the area of interest for uranium associations need further investigations using state-of-the-art to discover economic deposits for development and utilization of the resource. The result is the continuous of its mining work besides leachability experiments.

Acknowledgment

The authors would like to thank the late Prof. Dr. Mostafa E. Darwish and Dr. Reda El Arafy who kindly made available facilities.

References

1. Kusky TM, Abdelsalam M, Tucker R, Stern R (2003) Evolution of the East African and Related Orogens, and the Assembly of Gondwana. *Precamb Res* 123: 81-85.
2. Kröner A, Kruger J, Rashwan AA (1994) Age and tectonic setting of granitoid gneisses in the Eastern Desert of Egypt and south-west Sinai. *Geologische Rundschau* 83: 502-513.
3. Kusky TM, Ramadan TM (2002) Structural controls on Neoproterozoic mineralization in the South Eastern Desert, Egypt: an integrated field, Landsat TM, and SIR-C/IX SAR approach. *J Afr Earth Sci* 35: 107-121.
4. Stern RJ (1994) Arc assembly and continental collision in the Neoproterozoic East African Orogen: implications for the consolidation of Gondwanaland. *Ann Rev Earth Planet Sci* 22: 319-351.
5. Kampunzu AB, Kramers JD, Matutu MN (1998) Rb-Sr whole rock ages of the Lueshe, Kirumba and Numbi igneous complexes (Kivu, Democratic Republic of Congo) and the break-up of the Rodinia supercontinent. *J Afr Earth Sci* 26: 29-36.

6. Loizenbauer J, Wallbrecher E, Fritz H, Neumayr P, Khudeir AA, et al. (2001) Structural geology, single zircon ages and fluid inclusion studies of the Meatiq metamorphic core complex: Implications for Neoproterozoic tectonics in the Eastern Desert of Egypt. *Precamb Res* 110: 357-383.
7. Stern RJ (2002) Crustal evolution in the East African Orogen: a neodymium isotopic perspective. *J Afr Earth Sci* 34: 109-117.
8. Hargrove US, Stern RJ, Kimura JI, Manton WI, Johnson PR (2006) How juvenile is the Arabian-Nubian Shield? Evidence from Nd isotopes and pre-Neoproterozoic inherited zircon in the Bi'r Umq suture zone, Saudi Arabia. *Earth Planet Sci Lett* 252: 308-326.
9. Fritz H, Abdelsalam M, Ali KA, Bingen B, Collins AS, et al. (2013) Orogen styles in the East African Orogen: a review of the Neoproterozoic to Cambrian tectonic evolution. *J Afr Earth Sci* 86: 65-106.
10. El Ramly MF, Akaad MK (1960) The basement complex in the central eastern desert of Egypt between latitudes 24° 30' and 25° 40' N. *Geological survey of Egypt. Cairo, Egypt*.
11. El Gaby S (1975) Petrochemistry and geochemistry of some granites from Egypt. *Neues Jahrbuch für Mineralogie (Abhandlungen)* 124: 147-189.
12. Akaad MK, Noweir AM (1980) Geology and Lithostratigraphy of the Arabian Desert orogenic belt of Egypt between Lat. 25° 35' and 26° 30' N. *Inst Appl Geol Jeddah Bull* 4: 127-134.
13. Stern RJ, Hedge CE (1985) Geochronological and isotopic constraints on the Late Precambrian crustal evolution in the Eastern Desert of Egypt. *American Journal of Science* 285: 97-127.
14. Hassan MA, Hashad AH (1990) Precambrian of Egypt. In: Said R (Eds) *Geology of Egypt*. Balkema, Rotterdam, Netherlands.
15. Beyth M, Stern RJ, Altherr R, Kroner A (1994) The late Precambrian Timna igneous complex, southern Israel: evidence for comagmatic-type sanukitoid monzodiorite and alkali granite magma. *Lithos* 31: 103-124.
16. El Sayed MM (1998) Tectonic setting and petrogenesis of the Kadabora pluton: a late Proterozoic anorogenic A-type younger granitoid in the Egyptian Shield. *Chem Erde* 58: 38-63.
17. El Sayed MM (2003) Neoproterozoic magmatism in NW Sinai, Egypt: magma source and evolution of collision-related intracrustal anatectic leucogranite. *Int J Earth Sci* 92: 145-164.
18. Furnes H, El Sayed MM, Khalil SO, Hassanen MA (1996) Pan-African magmatism in the Wadi El Imra district, Central Eastern Desert, Egypt: geochemistry and tectonic environment. *J Geol Soc London* 153: 705-718.
19. El Shazly SM, El-Sayed MM (2000) Petrogenesis of the Pan-African El-Bula igneous suite, central Eastern Desert, Egypt. *J Afr Earth Sci* 31: 317-336.
20. Stern RJ (1979) Late Precambrian ensimatic volcanism in the Central Eastern Desert Egypt. *San Diego Univ, California, USA*.
21. Moghazi AM, Andersen T, Oweiss GA, El Bouseily AM (1998) Geochemical and Sr-Nd-Pb isotopic data bearing on the origin of Pan-African granitoids in the Kid area, southeast Sinai, Egypt. *J Geol Soc London* 155: 697-710.
22. El Sayed MM, Mohamed FH, Furnes H, Kanisawa S (2002) Geochemistry and petrogenesis of the Neoproterozoic granitoids in the Central Eastern Desert, Egypt. *Chem Erde* 62: 317-346.
23. Dahlkamp FJ (1993) *Uranium Ore Deposits*. Springer-Verlag Berlin Heidelberg, Berlin, Germany.
24. Bakhit FS (1978) Geology and radioactive mineralization of Gabal EL-Missikat area, Eastern Desert, Egypt. *Ain Shams University, Egypt*.
25. Assaf HS, Attawiya MY, Ibrahim ME, Ammar SE, Shalaby MH (1999) Geological, geochemical and mineralogical studies on the radioactive minerals occurrence at Qash Amir area, South Eastern Desert, Egypt. *J Mineral Soc Egypt* 11: 135-156.
26. Ibrahim ME, Zalata AA, Assaf HS, Ibrahim IH, Rashed MA (2005) El sella shear zone, southeastern Desert, Egypt; An example of vein-type uranium deposit. *Proceedings of 9th Inter Min Petrol and Metall Eng Conf, Cairo, Egypt*.
27. Ibrahim ME (1986) Geologic and radiometric studies on Um Ara granite pluton, south east Aswan, Egypt. *Monsoura University, Egypt*.
28. Roz ME (1994) Geology and uranium mineralization of Gebel Gatter area, North Eastern Desert, Egypt. *Al Azhar Univ, Egypt*.
29. Saleh GM (1993) Geologic and radiometric studies on the basement rocks of G. Nasb Aluba, southeastern Desert, Egypt. *Monsoura University, Egypt*.
30. Ibrahim ME, Saleh GM, Abd EL-Naby HH (2001) Uranium mineralization in the two mica granite of Gabal Ribdab area, South Eastern Desert, Egypt. *J Applied Radiation and Isotopes* 55: 861-872.
31. Ibrahim ME, Watanabe K, Saleh GM, Ibrahim WS (2015) Abu Rusheid lamprophyre dikes, South Eastern Desert, Egypt: as physical-chemical traps for REEs, Zn, Y, U, Cu, W, and Ag. *Arab J Geosci* 8: 9261-9270.
32. Finch R, Murakami T (1999) Systematic and paragenesis of uranium minerals. In: Burns PC, Finch R (Eds), *Uranium: Mineralogy, Geochemistry and the Environment*. *Reviews in Mineralogy* 38: 91-179.
33. Abdel Meguid AA (1986) Geologic and radiometric studies of uraniferous granite in Um Ara-Um Shilman area, south Eastern Desert, Egypt. *Suez Canal University, Egypt*.
34. Hussein HA, Zalata AA, Ibrahim ME (1986) Some radiometric studies on Um Ara granite pluton, south east Aswan, Egypt. *Bulletin of Faculty of Science, Monsoura University, Egypt*.
35. Dawood YH, Abd El-Naby HH (2001) Mineralogy and genesis of secondary uranium mineralization, Um Ara area, south Eastern Desert, Egypt. *Journal of African Earth Science* 32: 317-323.
36. Dawood YH (2001) Uranium-series disequilibrium dating of secondary uranium ore from south Eastern Desert of Egypt. *Applied Radiation and Isotopes* 55: 881-887.
37. Abd El Naby HH (2009) High and low temperature alteration of uranium and thorium minerals, Um Ara granites, south Eastern Desert, Egypt. *Ore Geology Reviews* 35: 436-446.
38. Zalata AA, Hussein HA, Ibrahim ME (1986) Some geological and petrochemical studies on alkali feldspar granites at Um Ara pluton, southeastern Desert, Egypt. *Bulletin of Faculty of Science, Monsoura University, Egypt*.
39. Abdalla HM (1996) Geochemical and mineralogical studies at Um Ara rare metals prospect, Southeastern Desert, Egypt. *Hokkaido University, Japan*.
40. Fawzy KM, El Shayip JB (2017) Mineralogy and radioactivity of anomalous sites of Wadi Murrah post-collision granites, south Eastern Desert, Egypt. *Arabian Journal of Geosciences* 10: 160-167.
41. Masuda A, Kawakami O, Dohmoto Y, Takenaka T (1987) Lanthanide tetrad effects in nature: two mutually opposite types, W and M. *J Geochem* 21: 119-124.
42. Saleh GM (2002) Neoproterozoic volcanism at Um Shilman-Um Dubr area, Southeast Aswan, Egypt: Geology, geochemistry and tectonic environment of the Dokhan Volcanic formation. *N Jb Miner Abh* 177: 321-347.
43. Meyer C, Hemley JJ (1967) *Wall rock alteration*, New York, USA.
44. Nesbitt HW, Young GM (1984) Prediction of some weathering trends of plutonic and volcanic rocks based up on thermodynamic and kinetic consideration. *Geochim Cosmochim Acta* 48: 1523-1534.
45. Nesbitt HW, Young GM (1989) Formation and diagenesis of weathering profiles. *J Geol* 97: 129-147.
46. Cuney M, Leroy J, Valdiviezo PA, Daziano C, Gamba M, et al. (1989) Geochemistry of the uranium mineralized Achala granitic complex, Argentina: Comparison with Hercynian peraluminous leucogranites of western Europe. *Metallogenesis of Uranium deposits* 20: 1-12. Vol. 32
47. Le Maitre RW, Bateman P, Dubek A, Keller J, Lameyre J, et al. (1989) A classification of igneous rocks and glossary of terms: Recommendations of the International Union of Geological sciences subcommission on the systematics of igneous rocks: Oxford, Black-well Scientific Publications, USA.
48. Large RR, Allen RL, Blacke MD, Herrmann W (2001) Hydrothermal alteration and volatile element halos for the Rosebery Klens volcanic-hosted massive sulfide deposit, Western Tasmania, *Economic Geology* 96: 1055-1072.
49. Ishikawa Y, Sowaguch T, Lwaya S, Horiuchi M (1976) Delineation of prospecting targets for kuroko deposits based on modes of volcanism of underlying dacites and alteration halos. *Mining Geology* 26: 105-117.
50. Date J, Watanabe Y, Saeki Y (1983) Zonal alteration around the Fukazawa Kuroko deposits, Akita Prefecture, Northern Japan. In: Hiroshi O(Eds) *The Kuroko and Related Volcanogenic Massive Sulfide Deposits*, Geoscience World, USA.

51. Eastoe CJ, Solomon M, Walshe JL (1987) District-scale alteration associated with massive sulfide deposits in the Mount Read Volcanics, Western Tasmania, *Economic Geology* 82: 1239-1258.
52. Lentz DR (1999) Petrology geochemistry and oxygen isotope interpretation of felsic volcanic and related rocks hosting the massive sulfide deposits, New Brunswick, Canada, *Economic Geology* 94: 57-86.
53. Schardt C, Cooke DR, Gemmill JB, Large RR (2001) Geochemical modeling of the zoned footwall alteration pipe, Hellyer volcanic-hosted massive sulphide deposit, western Tasmania, Australia: *Economic Geology* 96: 1037-1054.
54. Gifkins CC, Allen RL (2001) Textural and chemical characteristics of diagenetic and hydrothermal alteration in glassy volcanic rocks: Examples from the Mount Read volcanics, Tasmania. *Economic Geology* 96: 973-1002.
55. Taylor SR, McLennan SM (1985) *The Continental Crust: Its Composition and Evolution; An Examination of the Geochemical Record Preserved in Sedimentary Rocks*. Blackwell, Oxford, USA.
56. Rogers JJW, Adams JAS (1969) Thorium. In: Wedepohl KH (Eds) *Handbook of Geochemistry*. Springer-Verlag, Berlin, Germany.
57. Bea F (1996) Controls on the trace element composition of crustal melts. *Earth and Environmental Science Transactions of The Royal Society of Edinburgh* 87: 33-41.
58. Zhenhua Z, Masuda A, Shabani MB (1993) REE tetrad effects in rare-metal granites. *J Chin J Geochem* 12: 206-219.
59. Lee SG, Masuda A, Kim HS (1994) An Early Proterozoic leuco granitic gneiss with the REE tetrad phenomenon. *J Chem Geol* 114: 59-67.
60. Bau M (1996) Controls on the fractionation of isovalent trace elements in magmatic and aqueous systems: evidence from Y/Ho, Zr/Hf, and lanthanide tetrad effect. *Contributions to Mineralogy and Petrology* 123: 323-333.
61. Irber W (1999) The lanthanide tetrad effect and its correlation with K/Rb, Eu/Eu*, Sr/Eu, Y/Ho and Zr/Hf of evolving peraluminous granites. *Geochemica et Cosmochimica Acta* 63: 489-508.
62. Jahn BM, Wu F, Capdevila R, Martineau F, Zhao Z (2001) Highly evolved juvenile granites with tetrad REE patterns: the Woduhe and Baerzhe granites from the Great Xing and Mountains in NE China. *J Lithol* 59: 171-198.
63. Irber W, Forster HJ, Hech L, Moller P, Morteani G (1997) Experimental, geochemical, mineralogical and oxygen isotope constrain in the late magmatic history of the Fichtelgebirge granites (Germany). *Geol Rdsch* 86: 110-124.
64. Abdalla HM, Ishihara S, Matsueda H, Monem AA (1996) On the albite-enriched granitoids at Um Ara area, Southeastern Desert, Egypt. 1. Geochemical, ore potentiality and fluid inclusion studies. *Journal of Geochemical exploration* 57: 127-138.
65. Boynton WV (1984) *Cosmochemistry of the rare earth elements: meteorite studies*. Elsevier, USA. 32
66. Mansour SEI, El Afandy AH, Abdalla HM, Saleh GM, Abd El-Naby HH, et al. (2000) Uranium potentiality of Um Ara area, Southeastern Desert, Egypt. Internal report, Nuclear Materials Authority, Cairo, Egypt.

Author Affiliation

Top

Nuclear Materials Authority, El-Maadi, Cairo, Egypt

Submit your next manuscript and get advantages of SciTechnol submissions

- ❖ 80 Journals
- ❖ 21 Day rapid review process
- ❖ 3000 Editorial team
- ❖ 5 Million readers
- ❖ More than 5000 
- ❖ Quality and quick review processing through Editorial Manager System

Submit your next manuscript at • www.scitechnol.com/submission